Pressure broadening and shift of the cesium D_2 transition by the noble gases and N_2, H_2, HD, D_2, CH_4, C_2H_6, CF_4, and ^{3}He with comparison to the D_1 transition

Greg A. Pitz, Charles D. Fox, and Glen P. Perram*

Department of Engineering Physics, The Air Force Institute of Technology, 2950 Hobson Way, Wright-Patterson Air Force Base, Ohio, 45433-7765, USA

(Received 5 June 2010; published 8 October 2010)

The pressure broadening and shift rates for the cesium D_2 ($6\,^2P_{3/2} \leftarrow 6\,^2S_{1/2}$) transition with the noble gases and N_2, H_2, HD, D_2, CH_4, C_2H_6, CF_4, and ^{3}He were obtained for pressures less than 300 Torr at a temperature of 40°C by means of laser absorption spectroscopy. The collisional broadening rate γ_L for He, Ne, Ar, Kr, Xe, N_2, H_2, HD, D_2, CH_4, C_2H_6, CF_4, and ^{3}He are 20.59, 9.81, 16.47, 15.54, 18.41, 19.18, 27.13, 28.24, 22.84, 25.84, 26.14, 17.81, and 22.35 MHz/Torr, respectively. The uncertainty in the broadening rates is typically less than 0.3%. The corresponding pressure-induced shift rates δ are 0.69, −2.58, −6.18, −6.09, −6.75, −6.20, −4.83, −4.49, −4.54, −8.86, −9.38, −6.47, and 0.60 MHz/Torr with an uncertainty of less than 0.04 MHz/Torr. With the exception of diatomic collision partners, the broadening rates for Cs D_2 are 5%–15% less than the rates for Cs D_1. For light collision partners with a blue shift, the D_1 is shifted more than the D_2 line. The broadening cross sections for Cs and Rb are similar. However, the cross sections for K are about 70% larger and for Na, about 30% less.

DOI: 10.1103/PhysRevA.82.042502 PACS number(s): 32.70.Jz, 34.20.−b, 42.55.Xi, 42.62.Fi

I. INTRODUCTION

The efficiency and power scaling of solid-state lasers has been dramatically improved by replacing flash lamp excitation with high-power diode bars and stacks [1]. Extending the application of diode pumping to high-power gas-phase lasers offers improved thermal control of the gain medium and enhanced beam quality, but requires matching of the relatively broad spectral width of the diode pumps to the very narrow gas-phase absorption features. A prominent approach to such a system, the diode pumped alkali laser (DPAL), was demonstrated by Krupke *et al.* in 2003 and by Beach *et al.* in 2004 [2,3]. Indeed, the remarkable optical properties of the alkali metals allows for efficient phasing of many diodes via (1) optical exciation of the first $^2P_{3/2}$ state on the D_2 transition, (2) collisional relaxation to the spin-orbit split $^2P_{1/2}$ state, and (3) lasing back to the ground state along the D_1 transition. A single alkali-metal atom can be cycled in this system at rates exceeding 10^{10} s^{-1} [4].

Typical diode bars have a linewidth of ≈30 GHz requiring gas pressures of up to 10 atmospheres for efficient absorption. Recent success in narrow banding diode bars using external volume Bragg gratings appear to enable subatmosphere pressures for the DPAL system [5]. Alternatively, optically pumping transient alkali-metal–rare-gas molecules to the dissociative state which populates the upper laser level has also been recently demonstrated [6]. In all cases, the collision-induced broadening and shift of the alkali-metal D_1 and D_2 lines are key to laser performance. The ideal buffer gas in these laser systems should offer rapid spin-orbit relaxation rates, no quenching, and minimal reactivity, in addition to the effective line shape broadening. As part of a program to develop the spectroscopic and kinetic database for these lasers, we recently reported the collisional broadening and shifting of the D_1 line in Cs [7]. This paper reports on a continuation of this study for the pump transition on the Cs D_2 line.

The line shapes for the Cs D_2 transition have been studied in some detail from 1966 through 2008 [8–11]. The most accurate report using laser absorption spectroscopy is limited to helium and nitrogen collision partners [10]. The variations in the reported broadening and shifting rates are significant. For example, the reported broadening by Xe differs by more than 30 MHz/Torr [9,11]. Both blue and red shifts have been reported for He [8,11]. The reported rates for molecular collision partners is rather limited and the rates for methane, ethane, and tetrafluoromethane, key DPAL collision partners, are not available. The rates for ^{3}He have been predicted, but not observed [11].

A summary of the experimental observations regarding the broadening and shift rates for all the alkali-metal atoms offers several trends: (1) the broadening rates for D_2 lines are normally slightly greater than the D_1 line and (2) for blue shifts, the effect on the D_1 line is greater than the D_2 line [12]. The present work seeks to explore these trends for Cs by comparing the current results to our recent study of the D_1 line shapes [7].

II. EXPERIMENT

The apparatus for this experiment is similar to our recent report on the Cs D_1 line [7]. The coherent MBR-110 Ti:sapphire ring laser was tuned to the wavelength of the D_2 transition, 852 nm, and scanned 32 GHz. A Fabry-Perot etalon, with an approximately 300 MHz/free spectral range and held at room temperature, monitored the frequency of the scanning ring laser. The free spectral range of the etalon was calibrated for every scan by employing a cesium reference cell. The average free spectral range was 299.6 MHz. The ring laser provided up to 3 W with a linewidth less than 0.1 MHz and to avoid saturation broadening the beam was heavily attenuated to <1 μW. A trifurcated fiber bundle was employed to transport the beam and to randomize the polarization. One end of the fiber was focused through a 1 inch long low-pressure

*Glen.Perram@afit.edu
(937)255-3636 x4504

cell that was temperature controlled to 313 K as a frequency reference. A second branch of the fiber transmitted the light through another identical cell at the same temperature, where the pressure of the buffer gas was varied between 10 and 330 Torr. The final branch of the trifurcated fiber bundle monitored the incident laser power. The beam was amplitude modulated, at ≈1 kHz, and detected with Hamamatsu PhotoDiodes coupled to Stanford Research SRS850 lock-in amplifiers. Pressure was monitored with MKS capacitance manometers with an accuracy of 0.08%.

III. RESULTS

The hyperfine spectrum of the cesium D_2 transition is shown in Fig. 1(a), where the larger ground-state splitting (≈9.1926 GHz) is readily resolved. The Doppler width at $T = 313$ K is 386 MHz and the hyperfine splitting of the $^2P_{3/2}$ ranges from 151 to 251 MHz and is not resolved [13]. Figure 1(b) provides a simulation of the individual hyperfine structure of the $F'' = 3 \rightarrow F'' = 2$, 3, and 4 at a pressure of 10 Torr of nitrogen. The line shape profiles are broadened up to 6.32 GHz and shifted by as much as −2.08 GHz as the nitrogen is increased by 330 Torr. Each spectrum, which has an average signal to noise ratio of 700, was collected over 3 min and was sampled at over 100 000 spectral frequencies. The ground-state splitting of the D_2 transition is evident at all pressures observed in this study. The ground-state splitting therefore plays a significant role in the total line shape of both the D_2 and D_1 transitions even for pressures of an atmosphere [14]. Similar spectra were recorded for each of the buffer gases in this study. A blue shift was observed for only the lightest collisional partners, He and ^{3}He. The lightest molecular collisional partners H_2, HD, and D_2 induced a slight red shift, in contrast to the blue shifts observed previously for the D_1 transistion [7].

The full D_2 line is composed of six hyperfine components. The absorbance A is represented by a summation of Voigt profiles V for each component

$$A = -\ln\left(\frac{I}{I_0}\right) = c_0 + c_1\nu + c_2\sum_{i=1}^{6} a_i V(\nu_i + \delta\nu, \Delta\nu_L; \Delta\nu_D), \quad (1)$$

where ν_i is the line center frequency at zero pressure for the ith hyperfine component, $\delta\nu$ is the collision-induced shift common for all hyperfine components, $\Delta\nu_D = 386$ MHz is the Doppler width (full width at half maximum, FWHM) constrained at $T = 313$ K, $\Delta\nu_L$ is the Lorentzian width (FWHM), γ is the broadening rate, and P is the buffer gas pressure.

The absorbance is measured from the ratio of the transmitted intensities I and the incident intensities I_0. The absorbance is also defined as $A = \sigma l N$ where σ is the absorption cross section, $l = 2.5$ cm is the cell path length, and $n = 1.7 \times 10^{11}$ cm^{-3} is the Cs number density at 313 K. Due to the small vapor pressure of cesium, the self-broadening and shifts are assumed to be negligible (<1 kHz). A small linear baseline is accounted for with the fit constants $c_0 < 3.8 \times 10^{-3}$ and $c_1 < 1.44 \times 10^{-6}$ GHz^{-1}. Incident laser intensity was monitored via one leg of the trifurcated fiber bundle and largely eliminates the baseline. However, a small variation remains. The values for the background are similar to those found for the D_1 spectrum [7]. The relative line strengths of the hyperfine components a_i are constrained to the line shapes reported in Table I. The parameters for the numeric fit are limited to the collision-induced shift, the broadening rate, the absolute absorbance c_2, and the small baseline.

Examples of the nonlinear least-squares fit of Eq. (1) to three of the N_2 broadened spectra are shown in Fig. 2. The fit residuals are <8.1% across 55 Doppler widths, except in the core of the line shape at low pressures. The structured residuals at low pressure fade as pressure was increased beyond 80 Torr. Similar results were observed in our recent report of the Cs D_1 line and attributed to line narrowing by velocity changing collisions [7]. This effect was first observed by Dicke

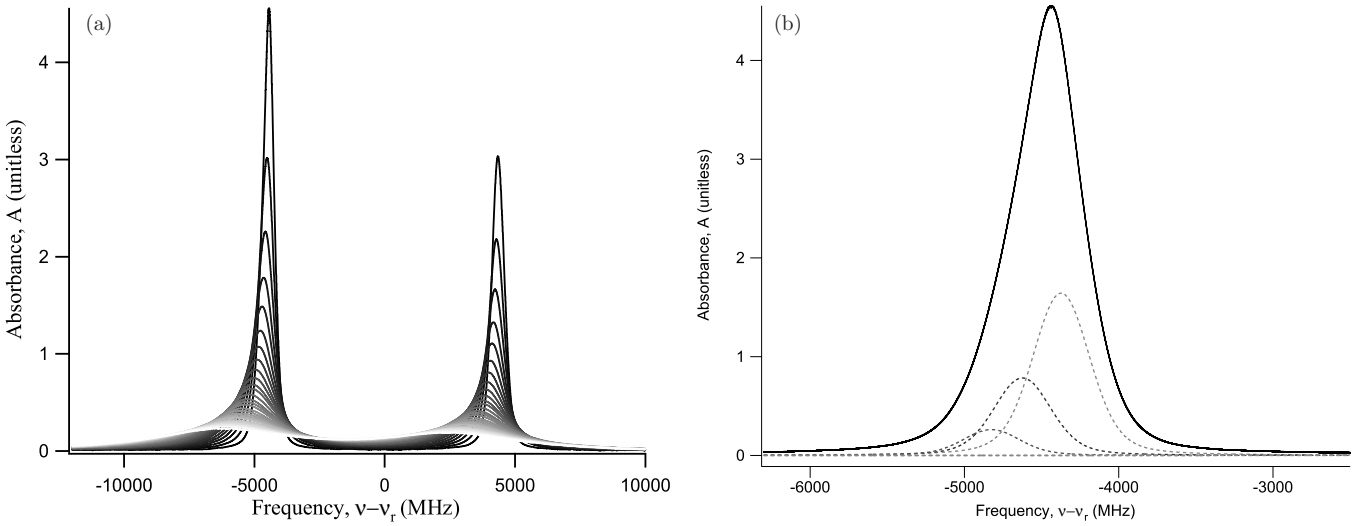

FIG. 1. (a) The observed cesium D_2 line shape pressure broadened by N_2 from 10 to 300 Torr and (b) simulation of components $F'' = 4$ to $F' = 3,4,5$ components with a set of data at low pressure.

TABLE I. Cesium hyperfine transition strengths for the D_2 transition.

Transition $S_{F\ F'}$	Relative line strengths, a_i (unitless)
$S_{4\ 5}$	11/18
$S_{4\ 4}$	7/24
$S_{4\ 3}$	7/72
$S_{3\ 4}$	15/56
$S_{3\ 3}$	3/8
$S_{3\ 2}$	5/14

in [15] and was numerically characterized by Galatry [15,16]. Neglecting this structure has a negligible effect on the Lorentzian widths and broadening rates [7,17].

The Lorentzian width and shift for each spectrum are plotted against their corresponding pressure of buffer gas in Figs. 3 and 4. The widths and shifts depend linearly on pressure

$$\Delta\nu_L = \gamma P + \gamma_N, \tag{2}$$

$$\delta\nu = \delta P, \tag{3}$$

where γ is the broadening rate for the buffer gas and γ_N is the known natural width for the D_2 transition 5.2 MHz [13]. The y intercept of Eqs. (2) and (3) were allowed to vary to account for

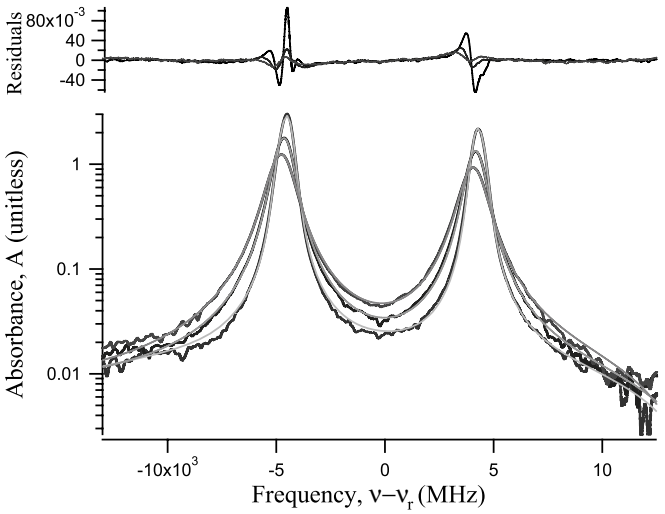

FIG. 2. A sample of the resultant fits with residuals to Eq. (1) for the D_2 transition under the influence of N_2 at 20, 40, and 60 Torr.

minor variations of the manometer. The resultant broadening γ and shift rates, δ with their corresponding slope-fit errors are shown in Tables II and III. The uncertainties were determined from the weighted least-square fit and reported as one standard deviation in the slope parameter. In addition, the pressure measurement of the capacitance manometer contributed an

TABLE II. Measured values for the broadening rate for the D_2 transition compared to the previous results.

Current work			Previous work			
Buffer gas	γ_1[a,b] (MHz/Torr)	$\frac{\gamma_{D_2}}{\gamma_{D_1}}$	T_2 (K)	γ_2 (MHz/Torr)	γ_{adj}[c] (MHz/Torr)	Ref.
He	20.59 ± 0.06	0.84	294	23.50 ± 0.21	22.77	[10]
			293	24.65 ± 0.26	23.84	[18]
			295	26.76 ± 1.69	25.97	[9]
			393	17.73 ± 0.75	19.87	[11]
^{3}He	22.35 ± 0.05	0.84	393	23.37 ± 1.132[d]	26.20	[11]
Ne	9.81 ± 0.06	0.90	293	12.39 ± 0.21	11.98	[18]
			295	10.34 ± 1.05	10.04	[9]
Ar	16.47 ± 0.18	0.90	293	19.91 ± 0.54	19.26	[18]
			295	22.78 ± 0.74	22.11	[9]
Kr	15.54 ± 0.05	0.87	295	16.83 ± 0.30	16.28	[18]
			295	10.94 ± 0.90	10.62	[9]
Xe	18.41 ± 0.07	0.93	295	17.22 ± 0.14	16.66	[18]
			295	57.56 ± 6.0	55.87	[9]
H_2	27.13 ± 0.2	1.27	295	59.66 ± 7.94	57.91	[9]
HD	28.24 ± 0.17	1.39	–	–	–	–
D_2	22.84 ± 0.16	1.26	–	–	–	–
N_2	19.18 ± 0.06	1.20	294	22.68 ± 0.20	21.98	[10]
			295	38.75 ± 9.57	37.61	[9]
			393	23.39 ± 1.51	26.21	[11]
CH_4	25.84 ± 0.09	0.86	–	–	–	–
C_2H_6	26.14 ± 0.08	0.95	–	–	–	–
CF_4	17.81 ± 0.05	0.94	–	–	–	–

[a]Error from a weighted linear fit only.
[b]$T_1 = 313$ K.
[c]See Eq. (4).
[d]Calculated value from ^{4}He.

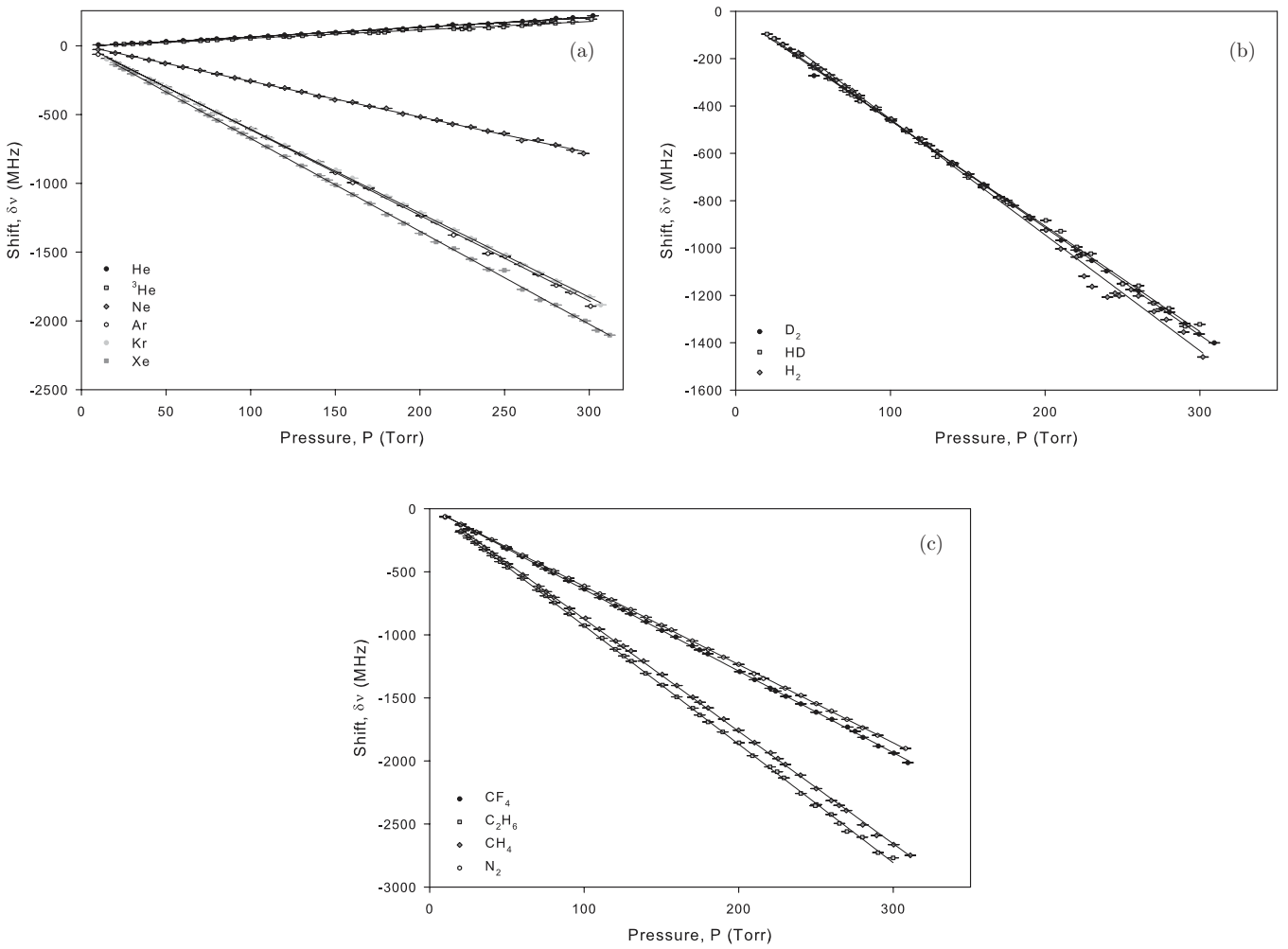

FIG. 3. Cesium D_2 hyperfine profile shift as a function of pressure of (a) the noble gases, (b) various hydrogen isotopes, and (c) several molecules.

uncertainty of about 0.08%. This resulted in the total error of ≈0.30%.

IV. DISCUSSION

The present results are compared with the previous measurement in Tables II and III. Prior studies were conducted at temperatures of $T_2 = 293$–393 K and the rates must be scaled to $T_1 = 313$ K for the present results. The temperature dependence of broadening rates are usually described as [19]

$$\gamma(T_2) = \gamma(T_1)\left(\frac{T_1}{T_2}\right)^n. \tag{4}$$

If the cross section σ is independent of the relative speed

$$\gamma(T) = \sigma\left(\frac{8k_bT}{\pi\mu}\right)^{1/2}, \tag{5}$$

then $n = \frac{1}{2}$ [7]. The relative speed $g = (\frac{8k_bT}{\pi\mu})^{1/2}$ depends on the reduced mass of the collision pair μ. The temperature dependence of the cross section was very weak for Cs D_1 and is assumed independent for the comparisons presented in Tables II and III [7]. For He, the present broadening results compare most favorably with the most recent result using broadband illumination and a grating spectrometer and not as closely with the similar laser absorption spectroscopy work [10,11]. The discrepancies between this work and that of Andalkar *et al.* could lie in the differences in the experimental procedures [10]. First, the prior work was limited to pressures under 160 Torr and only acquired under 16 data points for the calculation of the broadening rate. On the other hand, this work acquired data out to 300 Torr and had twice the number of data points. Second, in the calculation of the slope Andalkar *et al.* adjusted the widths by their laser linewidth and the natural width of the D_2 line to fit a line with a y intercept of zero. In contrast, due to small variations in the zeroing of the capacitance manometer between buffer gases, this work allowed the y intercept to vary allowing the slope to be fit more precisely. Finally, the fitting of the line by Andalkar *et al.* was a general least-squares fit but this work utilized the error of the Lorentzian width determined from the fitting of Eq. (1) to provide a relative weighting of the data and perform weighted least-squares fit. In the case of the N_2 and He rates of

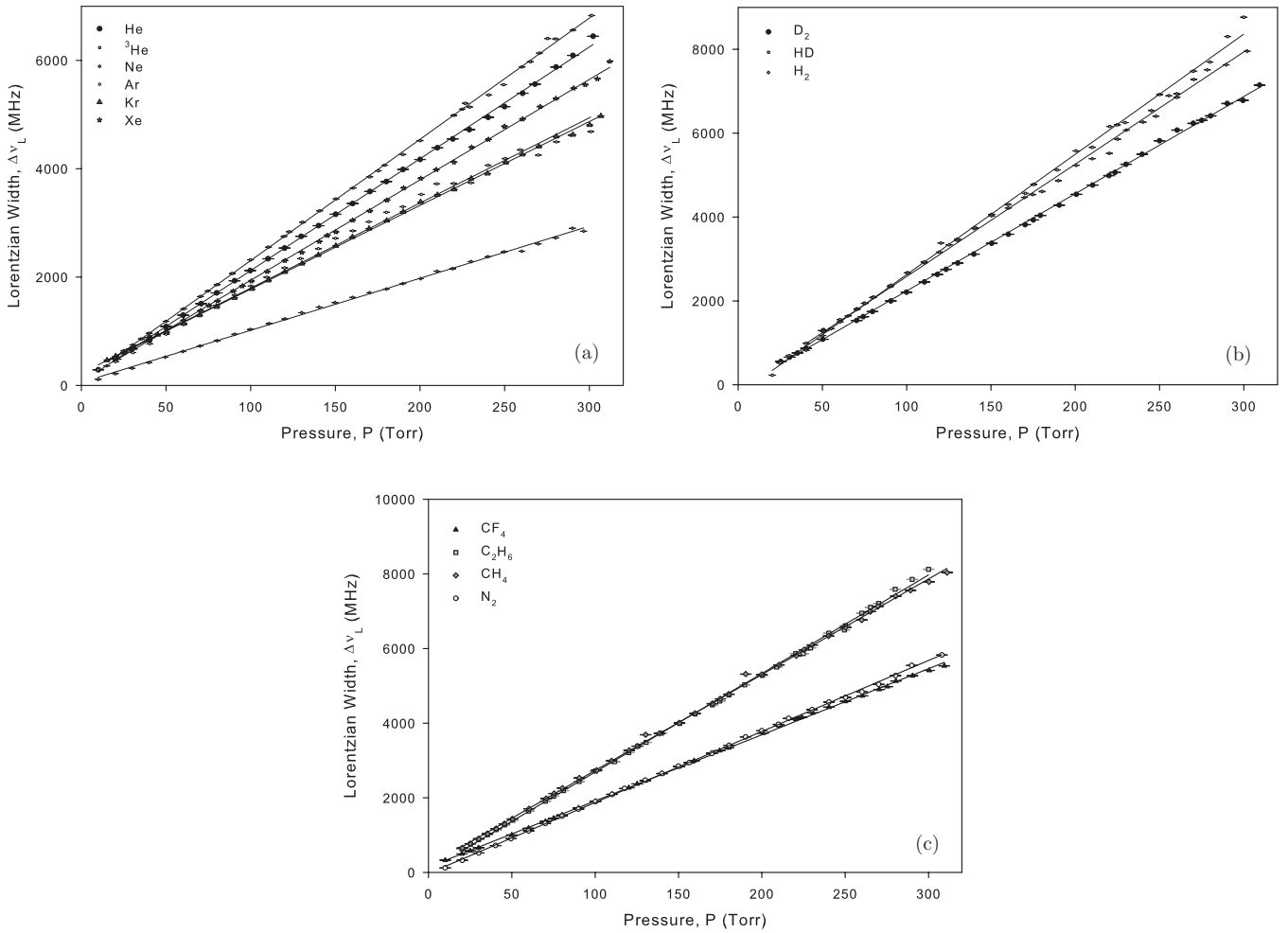

FIG. 4. Cesium D_2 hyperfine profile broadening as a function of pressure of (a) the noble gases, (b) various hydrogen isotopes, and (c) several molecules.

Andalkar *et al.* they are both approximately 10% greater than this work. However, for the recent work of Couture *et al.* the N_2 rate is 36% greater and the He rate is 4% less than that of this work. Additionally, the rates of Bernabeu and Alvarez are 96% greater for the N_2 rate and 26% greater for the He rate.

For the remainder of the rare gases, our results tend to favor the recent results using laser absorption techniques [18]. For Xe, N_2, and H_2 our results are two to three times smaller than the older work using scanning Fabry-Perot spectrometers [9]. Similar comparisons are observed for the shifting rates, with the notable exception of He. Our results agree with the small blue shift observed by Andalkar *et al.* and Inoue *et al.* and disagree with the larger blue shift of Bernabeu and Alvarez and the anomalous red shift of Couture *et al.* [9–11,18]. In the case of the red shift of Couture *et al.* this may be due to the extremely high temperatures of their study and the energy dependence of the shift cross sections. We also observe a blue shift of H_2 in disagreement with the Fabry-Perot results [9].

A comparison of the broadening and shifting of the D_1 and D_2 lines for Na, K, Rb, and Cs by a variety of collision partners is summarized in Fig. 5 [7,19–21]. In general, the rates are similar for the two spin-orbit split states. For Cs collisions with rare gases and large molecules the D_2 broadening rate is 5%–16% less than the D_1 rate. In contrast, Hindmarsh and Farr observed a slightly higher value for the D_1 lines when reviewing the full alkali-metal database in 1972 [12]. This conclusion is not supported when reviewing the more recent alkali-metal results.

Hindmarsh and Farr offered several additional observations regarding the shifting rates. First, the difference in the shift is dependent on the perturber and not on the nature of the alkali metal. This trend is supported by the data in Fig. 5. For example, the noble gases show that as the mass of the perturber is increased the shift switches direction and increases in magnitude. For the small number of molecules shown, no observable correlation is shown. Second, where there is a blue shift of the transition, the $^2P_{1/2}$ is greater than the $^2P_{3/2}$ rate. This is observed in Cs and Rb when mixed with He and ^{3}He. The collisional partner H_2, HD, and D_2 switch the direction they shift from blue to red when comparing $^2P_{1/2}$ to $^2P_{3/2}$. Third, the red shifts are typically small and there is no observable trend within the data. This statement is observed in Fig. 5(b). While there are more rates that are greater for $^2P_{3/2}$ there are still some that are greater for $^2P_{1/2}$.

TABLE III. Measured values for the shift rates for the D_2 transition compared to the previous results.

	Current work		Previous work		
Buffer gas	δ[ab] (MHz/Torr)	$\frac{\delta_{D_2}}{\delta_{D_1}}$	T_2 (K)	δ (MHz/Torr)	Ref.
He	0.69 ± 0.01	0.16	294	0.75 ± 0.01	[10]
			293	0.68 ± 0.03	[18]
			295	3.88 ± 1.68	[9]
			393	-1.40 ± 0.08	[11]
^{3}He	0.60 ± 0.01	0.10	393	-1.85 ± 0.11[c]	[11]
Ne	-2.58 ± 0.01	1.61	293	-2.59 ± 0.07	[18]
			295	-4.65 ± 0.30	[9]
Ar	-6.18 ± 0.02	0.96	293	-6.53 ± 0.16	[18]
			295	-7.65 ± 0.75	[9]
Kr	-6.09 ± 0.01	1.12	293	-6.44 ± 0.10	[18]
			295	-7.79 ± 1.05	[9]
Xe	-6.75 ± 0.01	1.05	293	-6.44 ± 0.1	[18]
			293	-13.34 ± 0.75	[9]
H_2	-4.83 ± 0.04	-4.25	295	1.65 ± 0.30	[9]
HD	-4.49 ± 0.03	-9.48	–	–	–
D_2	-4.54 ± 0.03	-5004	–	–	–
N_2	-6.2 ± 0.01	0.80	294	-6.73 ± 0.04	[10]
			295	-7.13 ± 0.24	[9]
			393	-6.79 ± 0.38	[11]
CH_4	-8.86 ± 0.02	0.93	–	–	–
C_2H_6	-9.38 ± 0.02	1.07	–	–	–
CF_4	-6.47 ± 0.01	1.06	–	–	–

[a]Error from a weighted linear fit only.
[b]$T_1 = 313$ K.
[c]Calculated value from ^{4}He.

A comparison of the effect of the alkali metal on the broadening cross section for the D_2 line is shown in Fig. 6. Each alkali metal shows a linear relationship between itself and that of cesium, but each has a different slope. The cross sections for Cs and Rb are similar. However, the cross sections

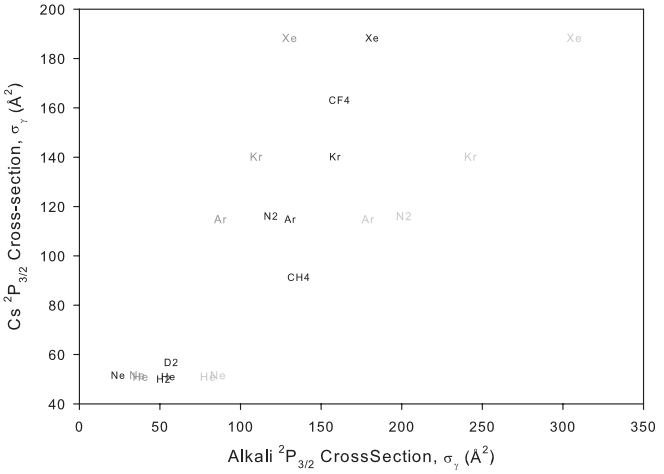

FIG. 6. Comparison between the $^2P_{3/2}$ broadening cross sections of Na (dark gray), K (light gray), and Rb with that of Cs.

for K are about 70% larger and for Na is about 30% less. Further study of the potential surfaces is required to explain the observed trends.

To further compare these rates, the Leonard-Jones interatomic potentials were calculated using the approach demonstrated by Hindmarsh and Farr and utilized by Rotondaro and Perram [7,12,21]. This approach assumes a 6–12 difference potential

$$V(R) = C_{12} r^{-12} - C_6 r^{-6}, \tag{6}$$

where r is the interatomic separation and C_6 and C_{12} are the coefficients for the r^{-6} and r^{-12} terms, respectively. These coefficients were determined from the broadening and shift rates using the impact approximation [22]. The impact approximation, while sufficient within the core of the Lorentzian profile, is inadequate in the far wings. In addition, these potentials average over all angles of impact and assume a single point of interaction between the alkali metal and the molecule. These interatomic difference potentials are shown in Fig. 7.

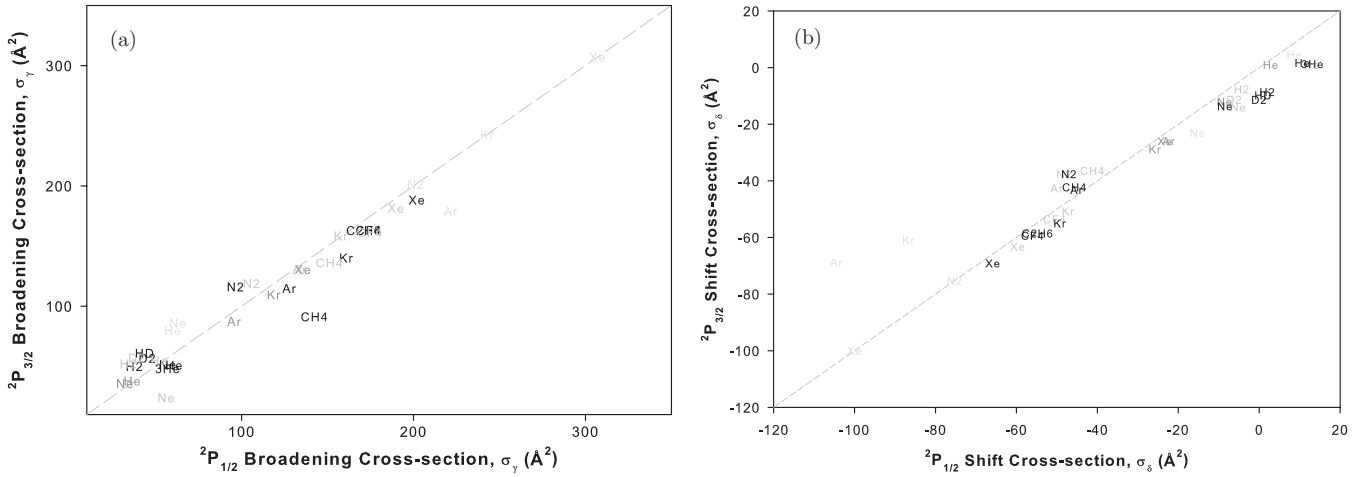

FIG. 5. The (a) collisional broadening and (b) shift cross section for the alkali metals Cs (■), Rb (■), K (■), and Na (■) with various collisional partners for the D_2 transition compared to the D_1. The rates were measured for Na by Kielkopf, for K by Lwin and McCartan, for Rb by Rotondaro and Perram, and Cs by Pitz *et al.* [7,19–21].

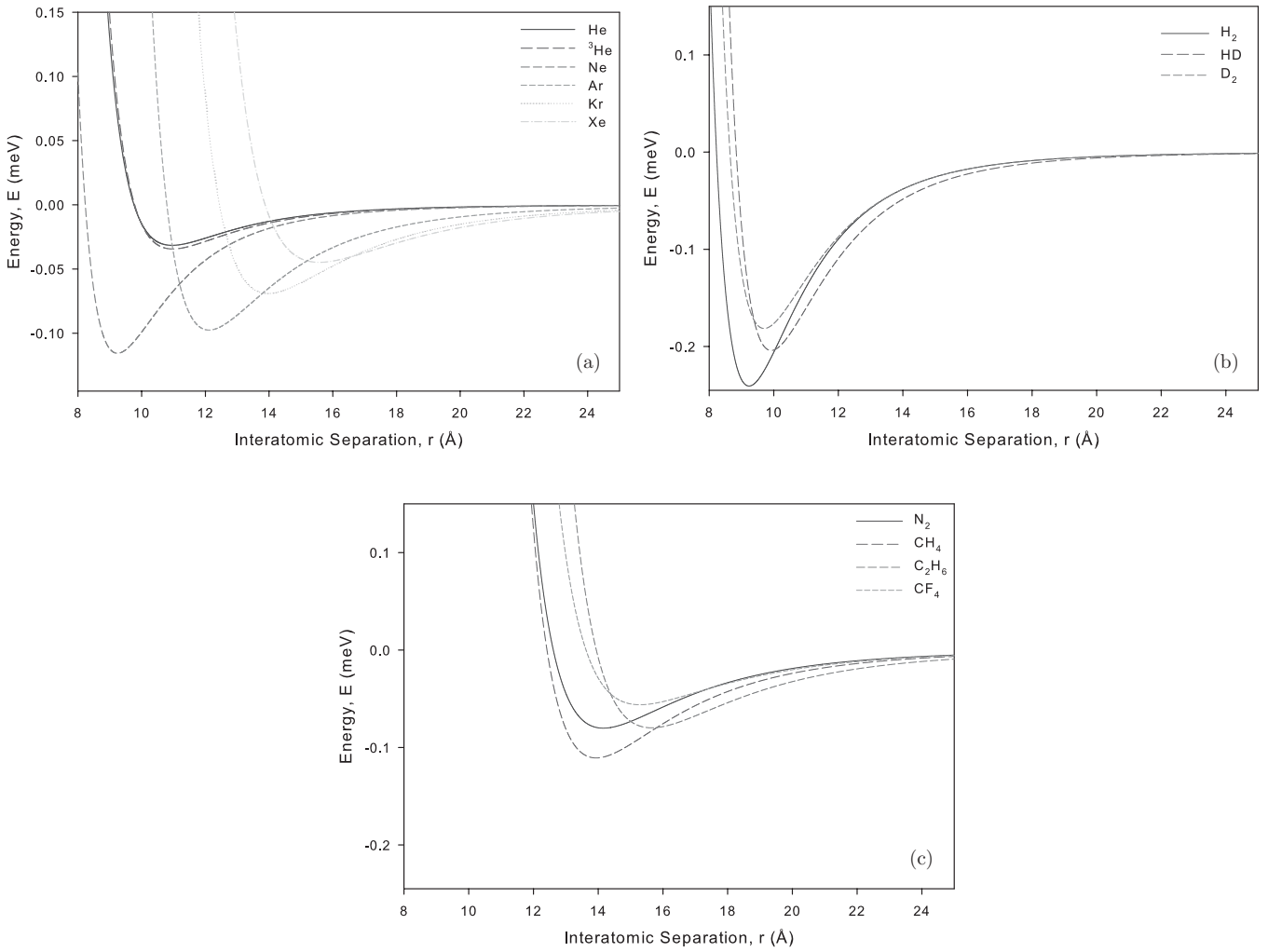

FIG. 7. The interatomic potential surfaces between Cs and (a) the noble gases, (b) various forms of hydrogen, and (c) an assortment of molecules.

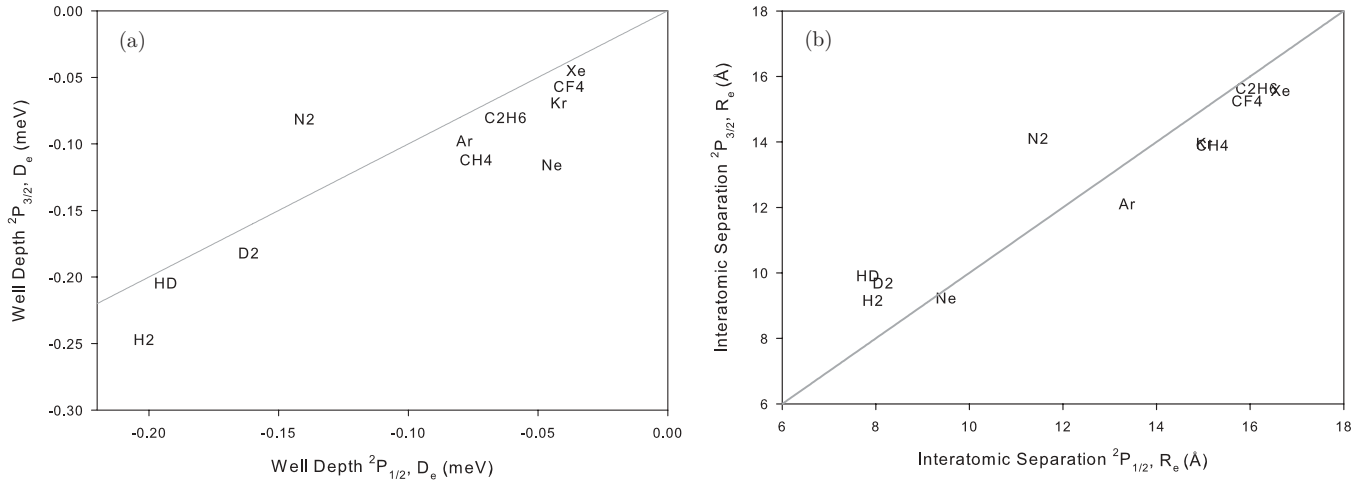

FIG. 8. Comparison between the (a) well depths and (b) the interatomic separation of cesium D_1 and D_2 transitions.

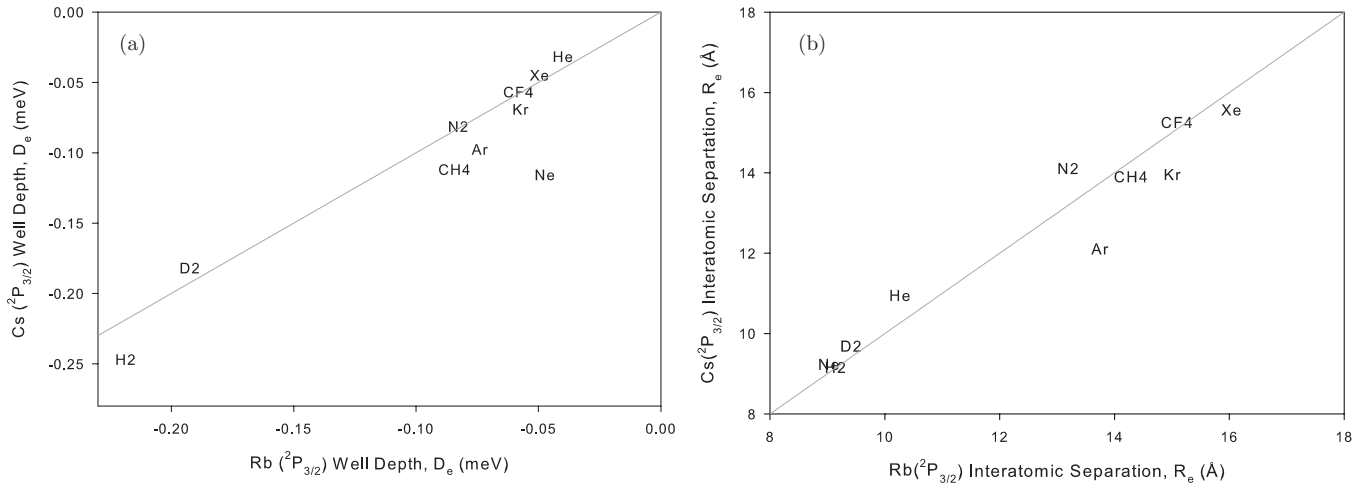

FIG. 9. Comparison between (a) the well depths and (b) the interatomic separation of cesium and rubidium.

Theoretical calculations of the ground-state potential energy surface for alkali-metal–rare-gas collision pairs, $X\,^2\Sigma$ and the excited states $A\,^2\Pi_{1/2}$ correlating to the separate $^2P_{1/2}$ atom and the $A\,^2\Pi_{3/2}$, $B\,^2\Sigma^+_{1/2}$ states correlating to the $^2P_{3/2}$, have been performed at various levels [23,24]. A comparison of these theoretical results to the interatomic difference potentials produced by the Hindmarsh and Farr techniques may show some striking differences. First, the excited state $^2P_{3/2}$ has been shown, by theoretical means, to split into two potential surfaces, $A\,^2\Pi_{3/2}$ and $B\,^2\Sigma^+_{1/2}$. The relative influence of the two surfaces on the D_2 line shape is unclear. Second, the quantitative values for the well depth and equilibrium interatomic separation distance are not similar between the two sets of potential surfaces. In the case of cesium-argon potential surfaces the theoretical values for the well depth are on the order of 60 meV, while the Hindmarsh and Farr surfaces are less than 0.1 meV [24]. In addition, the equilibrium interatomic separation for the theoretical surfaces is three times smaller than those obtained for this work [24].

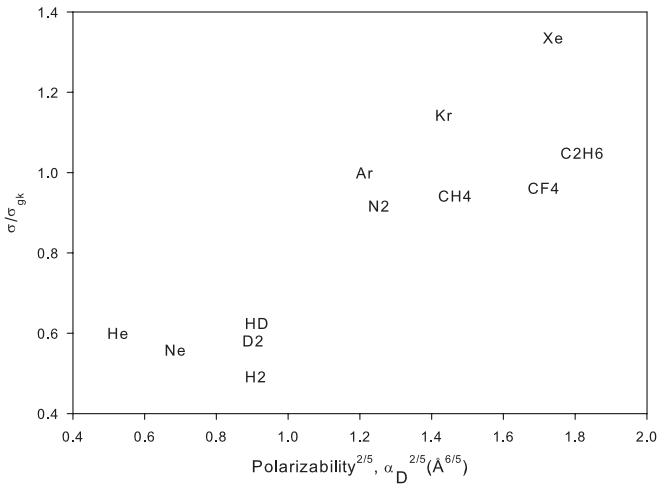

FIG. 10. Correlation of the probability for phase-changing collisions in the D_2 transition with dipole polarizability of the collision partner.

While these surfaces do not compare directly, if the Hindmarsh and Farr techniques are applied to other alkali metals the interatomic difference potentials that are obtained can be used to form additional correlations between alkali metals.

The equilibrium interatomic separation distance R_e and the well depth D_e, if they are bound surfaces, for the Cs D_1 and D_2 data are shown in Fig. 8. Well depth and equilibrium separation generally increase as the polarizability of the rare gas increases. Molecular hydrogen exhibits the strongest binding. The larger molecules behave similarly to the heavier rare gases. Nitrogen has a similar spin-orbit relaxation rate compared to the other diatomic molecules studied here, but the quenching rate is 11 times greater than H_2, HD, and D_2 [25]. This quenching rate for nitrogen is of the same order of magnitude for both the D_2 and D_1 transitions [25].

The values R_e and D_e for the cesium $^2P_{3/2}$ are also compared to the rubidium values calculated by Rotondaro and Perram, shown in Fig. 9 [21]. The values for D_e and R_e are strongly correlated between the two atoms with nitrogen being the largest outlier for both the well depth plot and the equilibrium separation.

The impact approximation and the Leonard-Jones potential suggests a correlation between the probability per collision for phase-changing collisions and polarizability. This present result is consistent with this prediction, as illustrated in Fig. 10. The ratio for the gas kinetic cross section

$$\sigma_g = \pi(r_{\mathrm{Cs}} + r_{\mathrm{buffergas}})^2, \tag{7}$$

were evaluated from Ref. [26]. The polarizability for the buffer gases was found in Ref. [27].

V. CONCLUSION

The rates for collision-induced broadening and shifting in the core of the Lorentzian profile for the Cs D_2 line with a broad range of collision partners at modest pressures has been determined with uncertainties of ≈0.3%. A number of trends in the broader alkali-metal database have been evaluated, but require further theoretical support for further interpretation.

Subatmospheric pressures are sufficient to broaden the pump transition for the Cs DPAL if diode bars and stacks can be narrowed to ≈30 GHz, as recent reports suggest [5]. The current addition of line shape data for ^{3}He, methane, and ethane allow detailed modeling of the bleached wave in recent laser demonstrations [3].

ACKNOWLEDGMENTS

Support for this work from the Air Force Office of Scientific Research and the High Energy Laser Joint Technology Office is gratefully acknowledged. We want to thank Nathan Zameroski for his help with the interatomic potentials.

[1] S. Lee, S. Kim, M. Yun, H. Kim, B. Cha, and H. Moon, Appl Optics **41**, 1089 (2002).
[2] W. Krupke, R. Beach, V. Kanz, and S. Payne, Opt. Lett. **28**, 2336 (2003).
[3] R. J. Beach, W. Krupke, V. Kanz, and S. Payne, J. Opt. Soc. Am. B **21**, 2151 (2004).
[4] W. Miller, Master's thesis, Air Force Institute of Technology, 2010.
[5] G. Venus, A. Gourevitch, V. Smirnov, and L. Glebov, in *SPIE Proceedings of Laser Source Technology for Defense and Security IV, Orlando, FL, 2008*, edited by M. Dubinskii and G. L. Wood (SPIE, Bellingham, WA, 2008), p. 69520D.
[6] J. D. Readle, C. J. Wagner, J. T. Verdeyen, D. L. Carroll, and J. G. Eden, in *SPIE Proceedings of High Energy/Average Power Lasers and Intense Beam Applications III, San Jose, CA, 2009*, edited by S. J. Davis, M. C. Heaven, and J. T. Schriempf (SPIE, Bellingham, WA, 2009), p. 71960D.
[7] G. A. Pitz, D. E. Wertepny, and G. P. Perram, Phys. Rev. A **80**, 062718 (2009).
[8] R. O. Garrett and S. Y. Ch'en, Phys. Rev. **144**, 66 (1966).
[9] E. Bernabeu and J. Alvarez, Phys. Rev. A **22**, 2690 (1980).
[10] A. Andalkar and R. B. Warrington, Phys. Rev. A **65**, 032708 (2002).
[11] A. H. Couture, T. Clegg, and B. Drieguys, J. Appl. Phys. **104**, 094912 (2008).
[12] W. R. Hindmarsh and J. M. Farr, Prog. Quantum Electron. **2**, 141 (1972).
[13] D. A. Steck [http://steck.us/alkalidata].
[14] G. A. Pitz and G. P. Perram, in *SPIE Proceedings of the 10th International Symposium on Gas Flow and Chemical Lasers, Taos, NM, 2008*, edited by C. R. Phipps (SPIE, Bellingham, WA, 2008), p. 700526.
[15] R. H. Dicke, Phys. Rev. **89**, 472 (1953).
[16] L. Galatry, Phys. Rev. **122**, 1218 (1961).
[17] K. J. Ritter and T. Wilkerson, J. Mol. Spectrosc. **121**, 1 (1987).
[18] Y. Inoue, K. Uchida, H. Hori, and T. Sakurai, J. Phys. Soc. Jpn. **59**, 516 (1990).
[19] J. F. Kielkopf, J. Phys. B **13**, 3813 (1980).
[20] N. Lwin and D. G. McCartan, J. Phys. B **11**, 3841 (1978).
[21] M. D. Rotondaro and G. P. Perram, J. Quant. Spectrosc. Radiat. Transfer **57**, 497 (1997).
[22] W. R. Hindmarsh and J. M. Farr, in *Progress in Quantum Electronics*, edited by J. Sanders (Pergamon, New York, 1972), pp. 145–153.
[23] L. A. Blank, G. S. Kedziora, and D. E. Weeks, in *SPIE Proceedings of High Energy/Average Power Lasers and Intense Beam Applications IV, San Francisco, CA, 2010*, edited by S. J. Davis, M. C. Heaven, and J. T. Schriempf (SPIE, Bellingham, WA, 2010), p. 75810I.
[24] J. M. Merritt, J. Han, T. Chang, and M. C. Heaven, in *SPIE Proceedings of High Energy/Average Power Lasers and Intense Beam Applications III, San Jose, CA 2009*, edited by S. J. Davis, M. C. Heaven, and J. T. Schriempf (SPIE, Bellingham, WA, 2009), p. 71960H.
[25] D. A. McGillis and L. Krause, Can. J. Phys. **46**, 1051 (1968).
[26] J. O. Hirschfelder, C. F. Curtiss, and R. B. Bird, *The Molecular Theory of Gases and Liquids* (Wiley, New York, 1954).
[27] H. L. Anderson, *A Physicist's Desk Reference* (American Institute of Physics, New York, 1989).